

Functional2Structural: Cross-Modality Brain Networks Representation Learning

Haoteng Tang¹, Xiyao Fu¹, Lei Guo¹, Yalin Wang², Scott Mackin³, Olusola Ajilore⁴, Alex Leow⁴, Paul Thompson⁵, Heng Huang¹, and Liang Zhan¹

¹ University of Pittsburgh, Pittsburgh, PA 15260, USA

² Arizona State University, Tempe, AZ 85281, USA

³ University of California San Francisco, San Francisco, CA 94143, USA

⁴ University of Illinois Chicago, Chicago, IL 60607, USA

⁵ University of Southern California, Los Angeles, CA 90007, USA

Abstract. MRI-based modeling of brain networks has been widely used to understand functional and structural interactions and connections among brain regions, and factors that affect them, such as brain development and disease. Graph mining on brain networks may facilitate the discovery of novel biomarkers for clinical phenotypes and neurodegenerative diseases. Since brain networks derived from functional and structural MRI describe the brain topology from different perspectives, exploring a representation that combines these cross-modality brain networks is non-trivial. Most current studies aim to extract a fused representation of the two types of brain network by projecting the structural network to the functional counterpart. Since the functional network is dynamic and the structural network is static, mapping a static object to a dynamic object is suboptimal. However, mapping in the opposite direction is not feasible due to the non-negativity requirement of current graph learning techniques. Here, we propose a novel graph learning framework, known as Deep Signed Brain Networks (DSBN), with a signed graph encoder that, from an opposite perspective, learns the cross-modality representations by projecting the functional network to the structural counterpart. We validate our framework on clinical phenotype and neurodegenerative disease prediction tasks using two independent, publicly available datasets (HCP and OASIS). The experimental results clearly demonstrate the advantages of our model compared to several state-of-the-art methods.

Keywords: Signed Graph Learning · Multimodal · Structural Network · Functional Network · Reconstruction · Prediction

1 Introduction

Recent years have witnessed great progress in applying graph theory to study MRI-derived brain networks, to discover novel biomarkers for clinical phenotypes or neurodegenerative diseases (e.g., Alzheimer’s disease or AD) [12,26,4]. Different MRI techniques can be used to reconstruct brain networks corresponding to different aspects of the brain organization or dynamics. For example, functional

MRI-derived functional networks provide measures of BOLD relationships over time between brain regions but not the existence of a physical direct link between these regions. By contrast, the diffusion MRI-derived structural network can describe the connectivity of white matter tracts between brain regions, yet does not inform us about whether this tract, or the regions it connects, are “activated” or “not activated” in a specific state. Therefore, these brain networks provide distinct but complementary information, and separately analyzing each of these networks will always be suboptimal.

Graph neural networks (GNNs) [17] have gained enormous attention recently. Although some progress [16,19] has been made by applying GNNs to brain networks, most existing techniques have been developed based on single-modality brain networks. It is well known that a high-level dependency, based on network communications, exists between brain structural and functional networks [24,3], which has motivated many studies [31,14,10] to integrate multimodal brain networks by constructing a projection between them using GNNs (e.g., [31]). Most existing studies [31,14,10] aim to reconstruct functional networks from brain structural counterparts. However, mapping a static object (structural network) to a dynamic one (functional network) is not optimal, even though the structural network may be better suited to serve as the template. Very few studies aim to construct the opposite mapping (i.e., from functional to structural networks); this may be because current GNNs can only encode unsigned graphs (i.e., structural networks in which all edge weights have non-negative values). The brain functional network is a signed graph by definition (including entries that denote negative correlations); as such, network edge weights can have negative values which will destroy the information aggregation mechanism in current GNNs.

To tackle this, we propose a new framework to encode signed graphs, and we apply this framework to project and encode brain functional networks to the corresponding structural networks. Our results demonstrate that the extracted latent network representations from this mapping can be used for clinical tasks (regression or classification) with better performance, compared with baseline methods. Our contributions are three-fold: (1) We propose an end-to-end network representation framework to model brain structural networks based on functional ones; this is the first work on this topic to the best of our knowledge. (2) We propose a signed graph encoder to embed the functional brain networks. (3) We draw graph saliency maps for clinical tasks, to enable phenotypic and disease-related biomarker detection and aid in interpretation.

2 Preliminaries of Signed Brain Networks

A brain network is an attributed and weighted graph $G = \{V, E\} = (A, X)$ with N nodes, where $V = \{v_i\}_{i=1}^N$ is the set of graph nodes representing brain regions, and $E = \{e_{i,j}\}$ is the edge set. $X \in \mathcal{R}^{N \times c}$ is the node feature matrix where $x_i \in \mathbb{R}^{1 \times c}$ is the i -th row of X representing the node feature of v_i . $A \in \mathbb{R}^{N \times N}$ is the adjacency matrix where $a_{i,j} \in \mathbb{R}$ represents the weights of the edge between v_i and v_j . In signed brain networks (i.e., functional brain networks), $a_{i,j} \in$

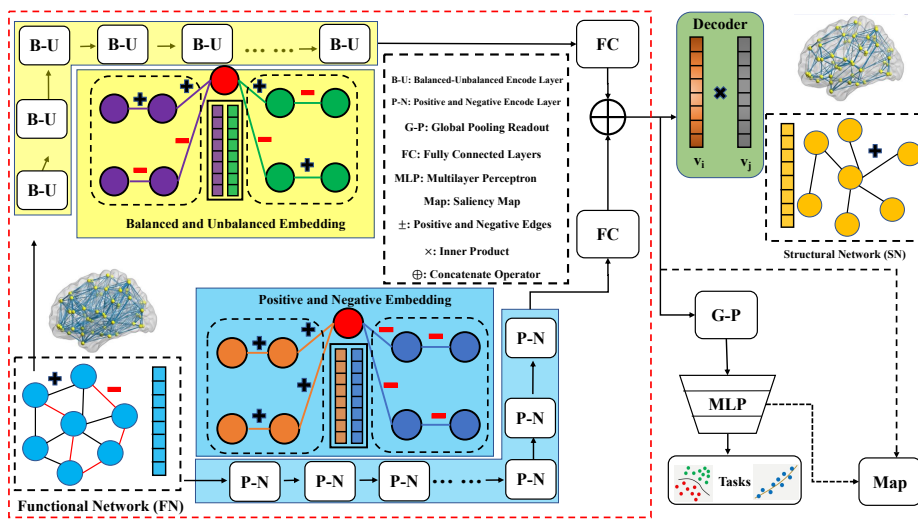


Fig. 1. Pipeline of the DSBN framework, including a signed graph encoder (in red dash box) scheme with two branches (BUE and PNE encoder heads in yellow and blue box) for functional network embedding, an inner-product decoder for structural network reconstruction and a downstream task branch for classification and regression.

$(-\infty, +\infty)$, while in unsigned brain networks (i.e., structural brain networks), $a_{i,j} \in [0, +\infty)$. We use $G^F = (A^F, X^F)$ and $G^S = (A^S, X^S)$ to represent the functional and structural brain networks, respectively. Given a specific node v_i in a signed network, we define their positive and negative neighbors set as \mathcal{N}_i^+ and \mathcal{N}_i^- , respectively. Following the balance theory [7,8,13,22], any node v_j belongs to the balanced set (denoted as Γ) of v_i if the path between v_i and v_j contains even number of negative edges. Otherwise, v_j belongs to the unbalanced set (denoted as Υ) of v_i .

3 Methodology

We first introduce the proposed multi-head signed graph encoder (SGE). Then, we present an end-to-end framework with the proposed encoder to reconstruct structural networks from functional networks and perform downstream tasks.

3.1 Signed Graph Encoder (SGE)

Our SGE consists of a balanced-unbalanced encoder (BUE) head and a positive-negative encoder (PNE) head. Motivated by the balance theory in Section 2, the BUE head encodes the graph node to the latent features with balanced and unbalanced components. Meanwhile, we split the signed graph into a positive sub-graph and a negative counterpart. The PNE head encodes these two sub-graphs

to generate the node latent features with positive and negative components. The yellow and blue boxes in Fig. 1 illustrate the BUE and PNE, respectively.

Balanced-Unbalanced Encoder (BUE). We use T to denote the encoder layer number and the $T - th$ layer of the encoder focuses on aggregating the $T - th$ hop neighbors of node v_i . To improve the generalization of local information aggregation in brain networks, a dynamic and fluctuating adjustment of aggregation weights (i.e., brain network edge weights) is arguably more reasonable and has been advocated during graph learning [31]. To this end, our BUE is designed based on the concept of graph attention [28].

Initial Layer ($T = 1$) We initialize balanced and unbalanced node latent feature components by:

$$x_i^{\Gamma(1)} = \sigma\left(\sum_{j \in \mathcal{N}_i^+} \alpha_{i,j}^{\Gamma(1)} x_j^{(0)} W^{\Gamma(1)}\right), \quad x_i^{\Upsilon(1)} = \sigma\left(\sum_{j \in \mathcal{N}_i^-} \alpha_{i,j}^{\Upsilon(1)} x_j^{(0)} W^{\Upsilon(1)}\right), \quad (1)$$

where σ is a nonlinear activation function. $x^{(0)} = x$ is input node features. $W^{\Gamma(1)}$ and $W^{\Upsilon(1)}$ are trainable weights to generate two latent feature components. $\alpha_{i,j}^{\Gamma(1)}$ and $\alpha_{i,j}^{\Upsilon(1)}$ are attention scores of brain nodes from the balanced and unbalanced set respectively. Following the work in [28], we first compute the attention coefficients by:

$$e_{i,j}^{\Gamma(1)} = a[x_i^{(0)} W^{\Gamma(1)}, x_j^{(0)} W^{\Gamma(1)}], \quad e_{i,j}^{\Upsilon(1)} = a[x_i^{(0)} W^{\Upsilon(1)}, x_j^{(0)} W^{\Upsilon(1)}] \quad (2)$$

where a is a trainable attentional weight vector and $[\cdot, \cdot]$ is a concatenation operator. Based on the attention coefficients, we derive the attention scores by:

$$\alpha_{i,j}^{\Gamma(1)} = \frac{\exp(e_{i,j}^{\Gamma(1)})}{\sum_{n \in \mathcal{N}_i^+} \exp(e_{i,n}^{\Gamma(1)})}, \quad \alpha_{i,j}^{\Upsilon(1)} = \frac{\exp(e_{i,j}^{\Upsilon(1)})}{\sum_{n \in \mathcal{N}_i^-} \exp(e_{i,n}^{\Upsilon(1)})} \quad (3)$$

Following Layers ($T > 1$) In the subsequent layers ($T > 1$), $x_i^{\Gamma(T)}$ and $x_i^{\Upsilon(T)}$ is generated by:

$$\begin{aligned} x_i^{\Gamma(T)} &= \sigma\left(\sum_{j \in \mathcal{N}_i^+, k \in \mathcal{N}_i^-} \alpha_{i,j}^{\Gamma(T)} x_j^{\Gamma(T-1)} W^{\Gamma(T)} + \alpha_{i,k}^{\Gamma(T-1)} x_k^{\Upsilon(T-1)} W^{\Gamma(T)}\right) \\ x_i^{\Upsilon(T)} &= \sigma\left(\sum_{j \in \mathcal{N}_i^+, k \in \mathcal{N}_i^-} \alpha_{i,j}^{\Upsilon(T)} x_j^{\Upsilon(T-1)} W^{\Upsilon(T)} + \alpha_{i,k}^{\Upsilon(T-1)} x_k^{\Gamma(T-1)} W^{\Upsilon(T)}\right) \end{aligned} \quad (4)$$

Similarly, we compute 4 attention coefficients as

$$\begin{aligned} e_{i,j}^{\Gamma(T)} &= a[x_i^{\Gamma(T-1)} W^{\Gamma(T)}, x_j^{\Gamma(T-1)} W^{\Gamma(T)}] \\ e_{i,k}^{\Gamma(T)} &= a[x_i^{\Upsilon(T-1)} W^{\Gamma(T)}, x_k^{\Upsilon(T-1)} W^{\Gamma(T)}] \\ e_{i,j}^{\Upsilon(T)} &= a[x_i^{\Upsilon(T-1)} W^{\Upsilon(T)}, x_j^{\Upsilon(T-1)} W^{\Upsilon(T)}] \\ e_{i,k}^{\Upsilon(T)} &= a[x_i^{\Gamma(T-1)} W^{\Upsilon(T)}, x_k^{\Gamma(T-1)} W^{\Upsilon(T)}] \end{aligned} \quad (5)$$

Then the 4 attention scores, $\alpha_{i,j}^{\Gamma(T)} = \exp(e_{i,j}^{\Gamma(T)}) / \sum_{\Gamma(T)}$, $\alpha_{i,k}^{\Gamma(T)} = \exp(e_{i,k}^{\Gamma(T)}) / \sum_{\Gamma(T)}$, $\alpha_{i,j}^{\Upsilon(T)} = \exp(e_{i,j}^{\Upsilon(T)}) / \sum_{\Upsilon(T)}$ and $\alpha_{i,k}^{\Upsilon(T)} = \exp(e_{i,k}^{\Upsilon(T)}) / \sum_{\Upsilon(T)}$, where $\sum_{\Gamma(T)} = \sum_{n \in \mathcal{N}_i} \exp(e_{i,n}^{\Gamma(T)})$ and $\sum_{\Upsilon(T)} = \sum_{n \in \mathcal{N}_i} \exp(e_{i,n}^{\Upsilon(T)})$.

After we obtain the two latent components, we concatenate them as the latent features generated by the BUE head by: $x_i^{BUE} = [x_i^{\Gamma}, x_i^{\Upsilon}]$.

Positive-Negative Encoder (PNE) We split the adjacency matrix of the functional network into positive and negative sub-network pairs (i.e., $G^{+F} = (A^{+F}, X)$ and $G^{-F} = (A^{-F}, X)$). For each sub-network, we forward it into T graph attention layers [28] to generate the positive and negative latent feature components (i.e., x_i^+ and x_i^-). As a result, the latent feature generated by the PNE head can be computed by $x_i^{PNE} = [x_i^+, x_i^-]$. The final fused latent features generated by our SGE can be computed by: $x_i = [x_i^{BUE}W, x_i^{PNE}W]$, where W is a set of trainable parameters to control feature dimensions.

3.2 Deep Signed Brain Networks (DSBN)

Our DSBN framework is illustrated in Fig. 1, which includes (1) a signed graph encoder (SGE) to generate the latent node features from brain functional networks, (2) a decoder to reconstruct brain structural networks from latent node features, and (3) Multilayer Perceptrons (MLP) for downstream tasks.

Structural Network Reconstruction and Downstream Tasks The structural network edges can be reconstructed by an inner-product decoder[18] as: $\hat{a}_{i,j}^S = \text{sigmoid}(x_i^T \cdot x_j)$, where the \cdot is an inner-product operator, \top is vector transpose.

We use a sum function as a global readout operator to obtain the whole graph representation (i.e., $X_G = \sum_{i=1}^N x_i$). Then, MLP are used to generate the final classification or regression output (i.e., $\hat{y} = MLP(X_G)$). Moreover, we use parameters in the last MLP layer and node latent features x_i to generate the brain network saliency map using the Class Activation Mapping (CAM) approach [23,2] for the classification task. The brain saliency map identifies the top-K most important brain regions associated with each class.

Loss Functions We summarize the loss functions here for our framework.

Reconstruction Loss The ground-truth brain structural network is sparse while the reconstructed structural network is fully connected. To facilitate network reconstruction, in the training stage, we add a small perturbation value (δ) to the edge weights of the ground-truth structural networks (i.e., $\hat{a}_{i,j}^S = a_{i,j}^S + \delta$) and build up the reconstruction loss as $\mathcal{L}_{recon} = \frac{1}{|E|} \sum_{i,j} (\hat{a}_{i,j}^S - \bar{a}_{i,j}^S)^2$, where $|E|$ is the number of edges.

Supervised Loss We deploy our framework on both regression and classification tasks. For the classification task, we use the negative log likelihood loss where $\mathcal{L}_{super} = NLLLoss(\hat{y}, y)$. For the regression task, we use L_1 loss where

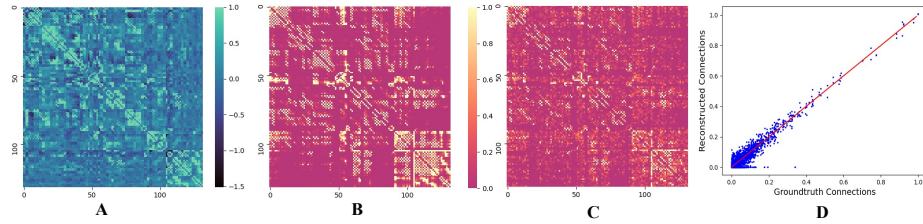


Fig. 2. Cross-modality learning results on the OASIS data. **(A)** is the averaged functional network, **(B)** and **(C)** are the mean reconstructed and ground-truth structural networks. **(D)** is to show that edge weights in the predicted structural network are significantly correlated with the ground truth data and $r = 0.917$ with $p = 0.0129$

$\mathcal{L}_{super} = L_1 Loss(\hat{y}, y)$. In summary, the overall loss function of the DSBN is $\mathcal{L}_{all} = \eta_1 \mathcal{L}_{recon} + \eta_2 \mathcal{L}_{super}$, where η_1, η_2 are loss weights.

4 Experiments

4.1 Data Description and Preprocessing

Two publicly available datasets were used to evaluate our framework. The first includes data from 1206 young healthy subjects (mean age 28.19 ± 7.15 , 657 women) from the Human Connectome Project [27] (HCP). The second includes 1326 subjects (mean age = 70.42 ± 8.95 , 738 women) from the Open Access Series of Imaging Studies (OASIS) dataset [20]. Details of each dataset may be found on their official websites. CONN [29] and FSL [15] were used to reconstruct the functional and structural networks, respectively. For the HCP data, both networks have a dimension of 82×82 based on 82 ROIs defined using FreeSurfer (V6.0) [11]. For the OASIS data, both networks have a dimension of 132×132 based on the Harvard-Oxford Atlas and AAL Atlas. We deliberately chose different network resolutions for HCP and OASIS, to evaluate whether the performance of our new framework is affected by the network dimension or atlas.

4.2 Implementation Details

The edge weights of the functional networks and structural networks were first normalized to the range of $[-1, 1]$ and $[0, 1]$, respectively. The node features are initialized as the min, 25%, median, 75%, max values of the fMRI bold signal. We randomly split each dataset into 5 disjoint sets for 5-fold cross-validations in the following experiments. The model is trained using the Adam optimizer with a batch size of 128. The initial learning rate is set to 0.001 and decayed by $(1 - \frac{current\ epoch}{max\ epoch})^{0.9}$. We also regularize the training with an L_2 weight decay of $1e^{-5}$. We stop the training if the validation loss does not improve for 100 epochs in an epoch termination condition with a maximum of 500 epochs, as was done in [21,25]. The experiments are deployed on one NVIDIA TITAN RTX GPU.

Table 1. Classification accuracy, precision, and F1-scores, with their standard deviation values under 5-fold cross-validation. The best results are highlighted in **bold** font.

Method	OASIS (Disease)			HCP (Gender)		
	Acc.	Prec.	F1	Acc.	Prec.	F1
t-BNE	57.84 ± 2.14	52.26 ± 2.39	55.17 ± 3.15	59.84 ± 2.05	57.77 ± 2.21	55.89 ± 1.96
MK-SVM	54.62 ± 3.33	49.86 ± 3.11	55.27 ± 4.15	58.21 ± 3.75	51.51 ± 2.84	59.19 ± 2.40
DIFFPOOL	66.29 ± 2.60	63.87 ± 2.14	69.91 ± 2.37	72.12 ± 1.81	68.84 ± 1.97	74.01 ± 2.16
SAGPOOL	64.53 ± 2.06	61.76 ± 2.99	68.97 ± 3.07	69.29 ± 1.84	70.18 ± 1.49	67.38 ± 1.12
BrainChey	69.26 ± 1.47	71.22 ± 1.95	70.46 ± 2.81	74.11 ± 2.05	76.26 ± 1.77	75.08 ± 2.60
BrainNet-CNN	73.37 ± 2.14	74.06 ± 1.59	73.27 ± 1.85	71.88 ± 1.69	70.18 ± 2.21	70.29 ± 2.10
DSBN w/o BUE	73.04 ± 3.03	74.74 ± 1.96	73.53 ± 2.23	78.15 ± 2.96	79.01 ± 1.68	80.47 ± 2.02
DSBN w/o PNE	75.38 ± 2.52	76.26 ± 2.96	78.68 ± 3.02	80.78 ± 2.44	81.16 ± 1.74	82.98 ± 2.01
DSBN w/o Recon.	75.94 ± 2.73	77.09 ± 2.52	75.46 ± 2.17	79.12 ± 2.06	80.55 ± 2.18	81.19 ± 1.96
DSBN	78.92 ± 1.38	79.81 ± 1.41	80.22 ± 2.25	82.19 ± 2.01	85.35 ± 1.99	84.71 ± 2.37

Table 2. Regression Mean Absolute Error (MAE) ± SD (standard deviation) under 5-fold cross-validation. The best results are highlighted in **bold** font.

	OASIS (MMSE)	HCP (MMSE)
tBNE	2.39 ± 0.74	2.17 ± 0.48
SAGPOOL	1.86 ± 0.27	1.55 ± 0.33
DIFFPOOL	1.69 ± 0.36	1.63 ± 0.14
BrainNet-CNN	1.40 ± 0.20	1.29 ± 0.06
BrainChey	1.12 ± 0.19	1.14 ± 0.25
DSBN w/o BUE	1.17 ± 0.22	1.11 ± 0.17
DSBN w/o PNE	1.06 ± 0.24	0.86 ± 0.34
DSBN w/o Recon.	0.97 ± 0.11	1.03 ± 0.19
DSBN	0.87 ± 0.18	0.69 ± 0.21

4.3 Brain Structural Network Reconstruction using DSBN

To show the performance of our DSBN on the reconstruction of brain structural networks, we train the model in a task-free manner where no task-specific supervised loss is involved. Since the δ value is set to 0.05 when we train the model, we set the reconstructed edge weights to 0 if the predicted weights are less than 0.05. The mean absolute error (MAE) values between the edge weights in the ground-truth and reconstructed networks are 0.074 ± 0.016 and 0.039 ± 0.058 under 5-fold cross-validation on the OASIS and HCP data, respectively. The reconstruction results on OASIS data are visualized in Fig. 2.

4.4 Disease and Sex Classification Tasks

Experimental Setup. 6 baselines were used for comparison, including 2 traditional graph embedding models (t-BNE [5] and MK-SVM [9]), 2 deep graph convolution models designed for brain network embedding (BrainChey [19] and BrainNet-CNN [16]), and 2 hierarchical graph neural networks with graph pooling strategies (DIFFPOOL [30] and SAGPOOL [21]) As mentioned above, the

baseline methods can only embed unsigned graphs. Therefore, we convert the functional networks to unsigned graphs by using the absolute values of the edge weights. Meanwhile, 3 variant models of our DSBN, including DSBN w/o BUE encoder, DSBN w/o PNE encoder and DSBN w/o reconstruction decoder, are evaluated for ablation studies. The number of BUE and PNE encoder layers is set to 3. We search the loss weights (details in [Supplementary](#)) η_1 and η_2 in the range of $[0.01, 0.1, 0.5, 1]$ and $[0.1, 1, 5]$ respectively, and determine the loss weights as $\eta_1 = 0.1$, $\eta_2 = 1$ for AD classification, $\eta_1 = 0.1$, $\eta_2 = 1$ for sex classification. The results are reported in terms of classification accuracy, precision and F1-scores, with their *std*.

Results Classification results for AD on OASIS and sex on HCP are presented in Table 1, which shows that our model achieves the best accuracy for both tasks, among all methods. For example, in the AD classification, our model outperforms the baselines with at least 7.6%, 7.8% and 9.4% increases in accuracy, precision and F1 scores, respectively. In general, the deep graph models perform better than the traditional graph embedding methods (*i.e.*, t-BNE and MK-SVM). When we abandon the cross-modality learning (*i.e.*, DSBN w/o Recon.), the performance, though comparable to baselines, decreases significantly. This shows the effectiveness of the cross-modality learning. The performance will also decrease when we remove BUE encoder or PNE encoder, which indicates that both balance and polarity properties are important for embedding functional networks. The brain saliency map is shown in [Supplementary](#) where we identify 10 key brain regions associated with AD (from OASIS) and with each sex (in HCP), respectively. The salient regions for females are concentrated in frontal regions of the brain while males have the opposite trend, consistent with the finding [6] that women are typically less aggressive than men, and, on average, less physically strong. For AD, most of the salient regions are located in subcortical structures, as well as the bilateral intracalcarine region, the caudate, and planum polare, which have been implicated as potential AD biomarkers [1].

4.5 MMSE Regression

Experimental Setup Mini-Mental State Exam (MMSE) is a quantitative measure of cognitive status in adults. In the MMSE regression task, the selected baselines for comparison (except for MK-SVM which is designed only for classification problems) and the structure of our DSBN remain unchanged. The loss weights are set to $\eta_1 = 0.5$ and $\eta_2 = 1$ for both datasets. Details of hyperparameter analysis are provided in the [Supplementary](#). The regression results are reported as average Mean Absolute Errors (MAE) with their *std*.

Results The MMSE regression results on the HCP and OASIS datasets are summarized in Table 2, which also demonstrates that our model outperforms all baselines. The regression results also indicate the superiority of the cross-modality learning and the importance of both BUE and PNE encoders.

5 Conclusion

We propose a novel multimodal brain network representation learning framework with a signed functional network encoder. The cross-modality network embedding is generated by mapping a functional brain network to its structural counterpart. The embedded network representations contribute to important clinical prediction tasks and the brain saliency map may assist with disease-related biomarker identification. We will explore the bijection between these two networks in the future.

References

1. Amoroso, N., La Rocca, M., Bruno, S., Maggipinto, T., Monaco, A., Bellotti, R., Tangaro, S.: Brain structural connectivity atrophy in alzheimer’s disease. arXiv preprint arXiv:1709.02369 (2017)
2. Arslan, S., Ktena, S.I., Glocker, B., Rueckert, D.: Graph saliency maps through spectral convolutional networks: Application to sex classification with brain connectivity. In: Graphs in biomedical image analysis and integrating medical imaging and non-imaging modalities, pp. 3–13. Springer (2018)
3. Bullmore, E., Sporns, O.: The economy of brain network organization. *Nature reviews neuroscience* **13**(5), 336–349 (2012)
4. Calhoun, V.D., Sui, J.: Multimodal fusion of brain imaging data: a key to finding the missing link (s) in complex mental illness. *Biological psychiatry: cognitive neuroscience and neuroimaging* **1**(3), 230–244 (2016)
5. Cao, B., He, L., Wei, X., Xing, M., Yu, P.S., Klumpp, H., Leow, A.D.: t-bne: Tensor-based brain network embedding. In: Proceedings of the 2017 SIAM International Conference on Data Mining. pp. 189–197. SIAM (2017)
6. Carlo, G., Raffaelli, M., Laible, D.J., Meyer, K.A.: Why are girls less physically aggressive than boys? personality and parenting mediators of physical aggression. *Sex Roles* **40**(9), 711–729 (1999)
7. Cartwright, D., Harary, F.: Structural balance: a generalization of heider’s theory. *Psychological review* **63**(5), 277 (1956)
8. Derr, T., Ma, Y., Tang, J.: Signed graph convolutional networks. In: 2018 IEEE International Conference on Data Mining (ICDM). pp. 929–934. IEEE (2018)
9. Dyrba, M., Grothe, M., Kirste, T., Teipel, S.J.: Multimodal analysis of functional and structural disconnection in a lzheimer’s disease using multiple kernel svm. *Human brain mapping* **36**(6), 2118–2131 (2015)
10. Finger, H., Bönstrup, M., Cheng, B., Messé, A., Hilgetag, C., Thomalla, G., Gerloff, C., König, P.: Modeling of large-scale functional brain networks based on structural connectivity from dti: comparison with eeg derived phase coupling networks and evaluation of alternative methods along the modeling path. *PLoS computational biology* **12**(8), e1005025 (2016)
11. Fischl, B.: Freesurfer. *Neuroimage* **62**(2), 774–781 (2012)
12. Hao, X., Xu, D., Bansal, R., Dong, Z., Liu, J., Wang, Z., Kangarlu, A., Liu, F., Duan, Y., Shova, S., et al.: Multimodal magnetic resonance imaging: The coordinated use of multiple, mutually informative probes to understand brain structure and function. *Human brain mapping* **34**(2), 253–271 (2013)
13. Heider, F.: Attitudes and cognitive organization. *The Journal of psychology* **21**(1), 107–112 (1946)

14. Huang, H., Ding, M.: Linking functional connectivity and structural connectivity quantitatively: a comparison of methods. *Brain connectivity* **6**(2), 99–108 (2016)
15. Jenkinson, M., Beckmann, C.F., Behrens, T.E., Woolrich, M.W., Smith, S.M.: *Fsl. Neuroimage* **62**(2), 782–790 (2012)
16. Kawahara, J., Brown, C.J., Miller, S.P., Booth, B.G., Chau, V., Grunau, R.E., Zwicker, J.G., Hamarneh, G.: Brainnetcnn: Convolutional neural networks for brain networks; towards predicting neurodevelopment. *NeuroImage* **146**, 1038–1049 (2017)
17. Kipf, T.N., Welling, M.: Semi-supervised classification with graph convolutional networks. arXiv preprint arXiv:1609.02907 (2016)
18. Kipf, T.N., Welling, M.: Variational graph auto-encoders. arXiv preprint arXiv:1611.07308 (2016)
19. Ktena, S.I., Parisot, S., Ferrante, E., Rajchl, M., Lee, M., Glocker, B., Rueckert, D.: Metric learning with spectral graph convolutions on brain connectivity networks. *NeuroImage* **169**, 431–442 (2018)
20. LaMontagne, P.J., Benzinger, T.L., Morris, J.C., Keefe, S., Hornbeck, R., Xiong, C., Grant, E., Hassenstab, J., Moulder, K., Vlassenko, A.G., et al.: Oasis-3: longitudinal neuroimaging, clinical, and cognitive dataset for normal aging and alzheimer disease. *MedRxiv* (2019)
21. Lee, J., Lee, I., Kang, J.: Self-attention graph pooling. In: International conference on machine learning. pp. 3734–3743. PMLR (2019)
22. Li, Y., Tian, Y., Zhang, J., Chang, Y.: Learning signed network embedding via graph attention. In: Proceedings of the AAAI Conference on Artificial Intelligence. vol. 34, pp. 4772–4779 (2020)
23. Pope, P.E., Kolouri, S., Rostami, M., Martin, C.E., Hoffmann, H.: Explainability methods for graph convolutional neural networks. In: Proceedings of the IEEE/CVF Conference on Computer Vision and Pattern Recognition. pp. 10772–10781 (2019)
24. Rusinek, H., De Santi, S., Frid, D., Tsui, W.H., Tarshish, C.Y., Convit, A., de Leon, M.J.: Regional brain atrophy rate predicts future cognitive decline: 6-year longitudinal mr imaging study of normal aging. *Radiology* **229**(3), 691–696 (2003)
25. Shchur, O., Mumme, M., Bojchevski, A., Günnemann, S.: Pitfalls of graph neural network evaluation. arXiv preprint arXiv:1811.05868 (2018)
26. Uludağ, K., Roebroek, A.: General overview on the merits of multimodal neuroimaging data fusion. *Neuroimage* **102**, 3–10 (2014)
27. Van Essen, D.C., Smith, S.M., Barch, D.M., Behrens, T.E., Yacoub, E., Ugurbil, K., Consortium, W.M.H., et al.: The wu-minn human connectome project: an overview. *Neuroimage* **80**, 62–79 (2013)
28. Veličković, P., Cucurull, G., Casanova, A., Romero, A., Lio, P., Bengio, Y.: Graph attention networks. arXiv preprint arXiv:1710.10903 (2017)
29. Whitfield-Gabrieli, S., Nieto-Castanon, A.: Conn: a functional connectivity toolbox for correlated and anticorrelated brain networks. *Brain connectivity* **2**(3), 125–141 (2012)
30. Ying, Z., You, J., Morris, C., Ren, X., Hamilton, W., Leskovec, J.: Hierarchical graph representation learning with differentiable pooling. *Advances in neural information processing systems* **31** (2018)
31. Zhang, W., Zhan, L., Thompson, P., Wang, Y.: Deep representation learning for multimodal brain networks. In: International Conference on Medical Image Computing and Computer-Assisted Intervention. pp. 613–624. Springer (2020)